Int. J. Heat Mass Transfer. Vol. 36, No. 3, pp. 599–610, 1993
Printed in Great Britain

0017–9310/93 $6.00 + 0.00

Experimental investigation on convective heat transfer of heated spinning sphere

SHENG MAO TIENG and AN CHERNG YAN
Institute of Aeronautics and Astronautics, National Cheng Kung University, Tainan, Taiwan 70101, R.O.C.

(*Received* 4 *October* 1991 *and in final form* 7 *April* 1992)

Abstract—The average Nusselt number of a heated sphere rotating in quiescent air was measured experimentally over the range $0 < Re < 33320$ from free to forced convection regimes. As well, real time holographic interferometry was applied to the observation of flows structure and evolution, and later employed to analyze the deviations revealed by a comparison of the measured data $\overline{Nu}$ with previous experimental and theoretical results. Thus, real time holographic visualization provides a physical understanding of the effect of the evoluting flow structure on $\overline{Nu}$ as rotational speed increases. In addition, a new asymptotic formula for correlating the experimentally measured $\overline{Nu}$ was established.

1. INTRODUCTION

THE PROBLEMS occurring in convective heat transfer over a heated rotating sphere have been the concern of researchers and engineers for more than 150 years [1–6]. Many authors concentrated on determining the average Nusselt number ($\overline{Nu}$) of the rotating sphere (an important parameter in describing the heat transfer characteristics), as well as the formulas of $\overline{Nu}$ correlating other physical parameters in different operating ranges. For instance, in free convection dominated flow, Yuge [7] experimentally measured $\overline{Nu}$ and obtained an empirical equation correlating $\overline{Nu}$ with the Grashof number (Gr). By assuming the flow around the sphere was laminar, Dorfman and Serazetdinov [8] theoretically determined a relation for $\overline{Nu}$ of a rotating sphere in the forced convection region

$$\overline{Nu} = 0.33 Re^{0.5} Pr^{0.4}. \tag{1}$$

Kreith *et al.* [9] correlated their experimental data by a similar relation to that of equation (1), but with a larger coefficient (0.43). This discrepancy in the coefficient may be due to the fact that Dorfman and Serazetdinov [8], in their theoretical analysis, neglected the effect of the eruption jet near the equatorial plane observed by Kreith *et al.* using smoke-visualization [9]. Banks [10], assuming the flow around the spinning sphere to be entirely laminar from the pole to the equator, obtained a correlation by numerical calculation of the same form as equation (1) but with a coefficient of 0.26, for $Pr = 0.7$. For large rotational Reynolds number ($5 \times 10^5 < Re < 7 \times 10^6$), the experimental results of Kreith *et al.* [9] were found to be correlated within a deviation of about 15% by the relation

$$\overline{Nu} = 0.066 Re^{0.67} Pr^{0.4} \begin{cases} Gr/Re^2 < 0.1 \\ 5 \times 10^5 < Re < 7 \times 10^6 \\ 0.7 < Pr < 7 \end{cases}. \tag{2}$$

In the mixed convection region, a relation correlating the experimental results was obtained by Nordlie and Kreith [11]. Churchill [12] proposed an asymptotic relation that correlated $\overline{Nu}$ with Gr and Re, while more recently Farouk [2], employing the full Navier–Stokes and energy equations along with the Boussinesq approximation, investigated the behavior of $\overline{Nu}$ in the mixed convection region.

Since, in rotating systems, convective heat transfer is closely related to the flow structure and its characteristics (which are usually very complex and unexpected), it offers real challenges to both theoreticians and experimenters alike [13]. Therefore, it is important not only to investigate such methods, equations and correlations that may be available for the determination of the heat transfer coefficient or Nusselt number, but also to explore new or unexpected physical phenomena in the convective flow which could considerably affect the heat transfer characteristics. New and advanced experiments are needed to push the limitations of existing experimental techniques, and extend the operating ranges in order to examine flow structure in more detail [13]. Unfortunately, most studies of convective flow structure have been confined to theoretical or numerical calculations, with very few being devoted to experimental visualization. To the best of the authors' knowledge, the experiment reported by Kreith *et al.* [9] may be the only one to have actually visualized the flow around a rotating sphere by using smoke-visualization. The presence of an eruption jet was noted near the equator in that experiment, but due to the limitations of the smoke method, more detailed phenomena were difficult to discern. In contrast, the optical interferometric technique is very sensitive to even slight changes in fluid density, and hence as a potential visualization technique, can provide more detailed information than more conventional methods.

In our recent research [14], the 3D-mixed convection flow around an inclined heated rotating sphere was investigated using diffuse-illumination holographic interferometry. Even though a few interesting

NOMENCLATURE

a	radius of sphere
B_i	Biot number
C_s	specific heat of sphere
C_p	specific heat of fluid at constant pressure
D_s	diameter of sphere
g	acceleration of gravity
Gr	Grashof number
h	heat transfer coefficient
K_s	thermal conductivity of sphere
K_f	thermal conductivity of fluid
L_s	characteristic length of sphere, volume/surface area
$\overline{Nu}$	average Nusselt number
$\overline{Nu}_f$	average Nusselt number for forced convection
$\overline{Nu}_N$	average Nusselt number for free convection
Pr	Prandtl number
Re	rotational Reynolds number
T_f	film temperature, $(T_s+T_\infty)/2$
T_∞	ambient temperature
T_s	temperature of sphere.

Greek symbols

β	thermal coefficient of volume expansion
ε	emissivity
μ	fluid viscosity
ν	fluid kinematic viscosity, μ/ρ
ρ	density of air
σ	Stefan–Boltzman radiation constant
Ω	angular velocity of sphere [rad s^{-1}].

flow phenomena were observed, the holographic technique used in that work was based on a double exposure method which captures transient phenomena very well, but cannot effectively examine continuously evolving processes in the flow. Therefore, in this work, real time holographic interferometry will be set up in order to observe the evolution of the flow as rotating speed is increased.

In addition, the average Nusselt number of a heated rotating sphere will be measured during cooling tests over a wide range of Reynolds numbers ($Re = 0$–33 320), from free, to mixed, to forced convection. The effect of flow structure on the behavior of $\overline{Nu}$ in different convective regimes will be analyzed and discussed based on the real time holographic visualizations, as well as a comparison of the measured data with previous experimental results and theoretical predictions.

2. TECHNIQUE AND INSTRUMENTATION

2.1. *Test apparatus*

A schematic diagram and photograph showing the test apparatus used for this experiment are given in Figs. 1(a) and (b), respectively. The test sphere is made of chrome steel (diameter 35 mm), and was rotated by a d.c.-motor with variable speed capability. The rotational shaft supporting the sphere (diameter 4 mm; length 30 mm) was designed to be as small as possible in order to minimize heat conduction along it. The temperature of the sphere was measured by a micro-thermocouple which was inserted into the sphere center through a hole (diameter 2 mm; depth 20 mm) aligned along the rotational axis in opposition to the shaft (see Fig. 1(a)). Thus, when the sphere rotated, the thermocouple did not. Moreover, as the thermocouple did not touch the hole wall, the effects of friction between the thermocouple junction and the hole can be neglected. The hole opening was blocked by asbestos for heat insulation.

2.2. *Measurements of the average Nusselt number*

Conventionally, for an isothermal sphere rotating in an otherwise quiescent fluid, the overall average heat transfer coefficient $\bar{h}$ is the sum of the average convective heat transfer coefficient $\bar{h}_c$ and the radiation heat transfer coefficient $\bar{h}_r$. However, due to the low test temperature (260–300°C) $\bar{h}_r$ was so small compared with $\bar{h}_c$ as to be ignorable. Therefore, it was assumed $\bar{h} \approx \bar{h}_c$, which was determined by means of a transient technique described in refs. [9, 11]

$$\bar{h} \approx \bar{h}_c = \frac{(4/3)\pi a^3 \rho_s C_s (\mathrm{d}T_s/\mathrm{d}t)}{4\pi a^2 (T_s - T_\infty)} = \frac{C_s \rho_s a}{3}\left[\frac{\mathrm{d}T_s(t)/\mathrm{d}t}{T_s(t) - T_\infty}\right]. \quad (3)$$

This equation implies that $\bar{h}$ can be obtained in cooling tests by measuring the slope of the sphere temperature decay curve at the test temperature point. Then, the average Nusselt number can be calculated according to the following relation [9]:

$$\overline{Nu} = \frac{\bar{h} D_s}{K_f}. \quad (4)$$

In this work, the sphere was assumed to be a lumped system, the temperature distribution within the sphere at any instant being regarded as almost uniform (i.e. the temperature gradients within the sphere can be neglected). According to ref. [15] the criterion for the lumped system approximation is that the Biot number remains less than about 0.1, that is, if

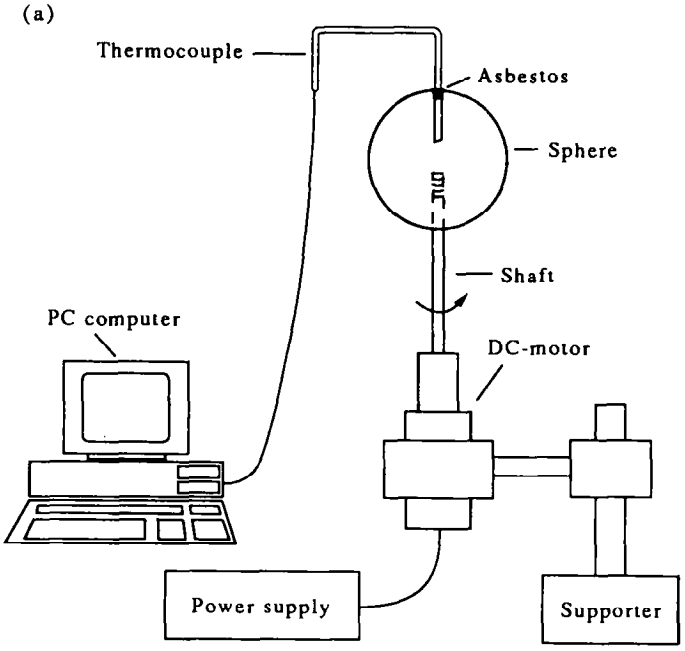

(b)

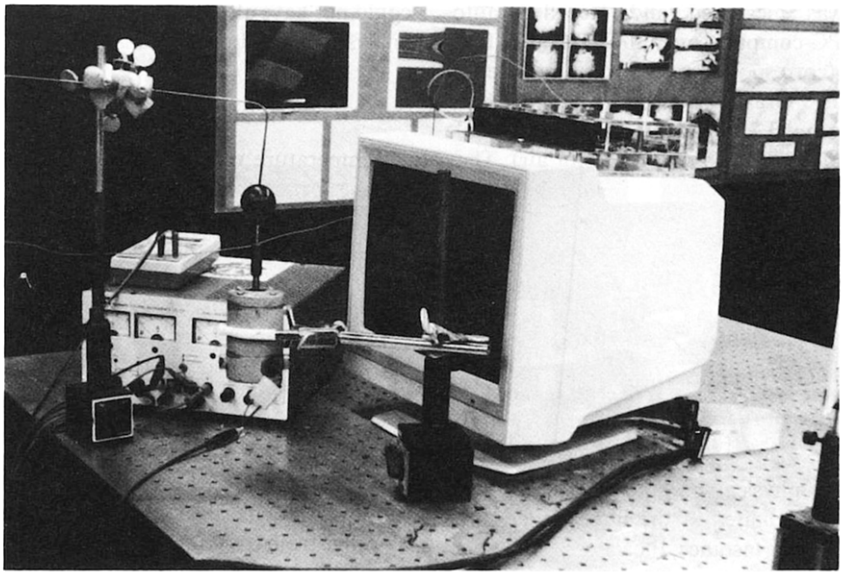

FIG. 1. (a) Schematic diagram of test apparatus; (b) photograph of test apparatus.

$$B_i = \frac{L_s/K_s}{1/h} = \frac{\text{specific internal resistance to heat flow across } L_s}{\text{specific skin resistance to heat flow at the outer surface}} < 0.1 \quad (5)$$

where

$$L_s = \frac{\text{volume}}{\text{surface area}} = \frac{a}{3} = \frac{1.75 \times 10^{-2}}{3}\ \text{m}$$

$h = 50\ \text{W m}^{-2}\ ^\circ\text{C}^{-1}$ (at 300°C); (at $Re = 33\,320$, according to equation (1)); $K_s = 47\ \text{W m}^{-2}\ ^\circ\text{C}^{-1}$ (at 300°C and $Cr = 1\%$) [16]. Thus,

$$B_i = \frac{50 \times (1.75 \times 10^{-2}/3)}{47} = 0.0063 \ll 0.1.$$

Since the sphere in this study can be considered a

lumped system, its surface temperature was measured only at one location, as shown in Fig. 1.

It is found that the temperature differences within a solid remain less than about 5% of the center temperature if $B_i < 0.1$ [16]. The local surface temperatures was simultaneously measured with thermocouples during cooling if the sphere and the data differences between all the measured points were within 3–5°C. These measurements were made for the case of a stationary sphere and the thermocouples were in tight contact with the sphere surface. In addition, we also measured temperatures at different points along the hole axis using different rotational speeds. In all these cases, the measured data differences remained less than 5% of the sphere center temperature (15°C). In fact, they were all within 2–3°C of each other.

The signals of the thermocouple were processed and averaged by an A/D converter, amplifier, data scanning circuit and 80286-based computer. The sampling time is 0.1 s. During the experimentation process, the sphere was first heated by a burner to a temperature 30°C higher than that desired (260 and 300°C). The flame was then taken away, and the sphere rotated at the required speed. During rotation, the decreasing temperature was measured and recorded automatically by a PC-computer over a *Re* test range from zero to 33 320 (corresponding to a rotating speed of 0–7000 rpm). The Grashof numbers were 3.07×10^5 (at $T_s = 260$°C) and 3.21×10^5 (at $T_s = 300$°C), while the Prandtl number was taken as 0.72 (for air). They are defined, respectively, as

$$Re = \frac{\rho \Omega D^2}{\mu} \tag{6}$$

$$Gr = \beta g (T_s - T_\infty) \frac{D^3}{\nu^2} \tag{7}$$

$$Pr = \mu \frac{C_p}{K_f}. \tag{8}$$

Note that, all physical parameters used in this experiment were evaluated at the film temperature; $T_f = (T_s + T_\infty)/2$. For instance, the values of $g\beta/\nu^2$ (in equation (7)) and K_f (in equations (4) and (8)) were taken as 30×10^6 K^{-1} m^{-3} and 0.0347 W m^{-1} K^{-1} [17], respectively, where $T_f = (570 + 300)/2 = 435$ K.

2.3. *Real time holographic interferometry*

In this experiment, real time holographic interferometry [18] was employed in order to visually analyze the process of flow evolution as the rotating speed of the sphere was increased from free to forced convection. The advantage of this technique lies in its capability of *in situ*, continuous observation of the changing process, whereas the double exposure technique is able to capture only transient phenomena in the evolution process. A schematic diagram and photograph of the optical system used are shown in Figs. 2(a) and (b), respectively. A single frequency Ar^+ laser with an output of 1.2 W and a wavelength of 5145 Å (Innova 306, Coherent Inc.) was employed as the light source. The hologram plate was an HC-320 thermoplastic recorder (Newport Inc.) which can be automatically processed *in situ* by an HC-320 controller. The hologram was exposed once while the stationary sphere was at ambient temperature, and subsequently developed *in situ*. The plate was then illuminated by the original reference beam, while, the object beam illuminated the rotating sphere. The changing fringe pattern, corresponding to the evolution of the flow can be observed through the plate with the naked eye, or recorded on a video-camera. For details of this technique, the reader is referred to refs. [18, 19].

It should be pointed out that in order to minimize the temperature decrease during the real time observation process, the total evolutionary process (in our case, *Re* from 0 to 15 000) was divided into three observation steps (i.e. *Re* = 0–5000; 5000–10 000; 10 000–15 000). For each step, the observation period was only about 1 min. As the duration of observation was so short, the temperature of the spinning sphere decayed only 20–30°C, and thus the Grashof number could not have altered enough to effect the qualitative analyses of the flow visualization.

3. RESULTS AND DISCUSSION

Temperature variation during the cooling process vs time for the rotating isothermal sphere at different rotational speeds was measured by the thermocouple, and the results are plotted in Fig. 3. The values of dT_s/dt at different surface temperatures ($T_s = 260$ and 300°C) were directly determined by measuring the slopes of the curves, whereas the average Nusselt numbers were calculated according to equation (4). The results are listed in Table 1, and plotted as a function of *Re* in Fig. 4.

From Fig. 4, it is evident that the average Nusselt number does not begin to quickly increase until the rotational Reynolds number approaches 9000. In the *Re* range from 0 to 1000, $\overline{Nu}$ changes very slightly and essentially remains constant. Then, as the rotational rate is increased further, $\overline{Nu}$ begins to gradually rise along a curved path until a transition point at $Re = 9000$ is reached, after which $\overline{Nu}$ increases quickly and in a linear fashion. Similar functional relationships of $\overline{Nu}$ vs *Re* were also predicted theoretically by Farouk [2], and are plotted (dotted lines) for comparison with the experimental values (solid lines) in Fig. 4. Although the results were obtained at different Grashof numbers (i.e. $Gr = 1.39 \times 10^3$, 1.39×10^4, 1.39×10^5 in the case of Farouk, and $Gr = 3.07 \times 10^5$, 3.21×10^6 in the present work), the curves exhibit the same tendencies. This $\overline{Nu}$ behavior can be most readily understood by analyzing the real time holographic visualization.

A photographic camera was used to visualize the

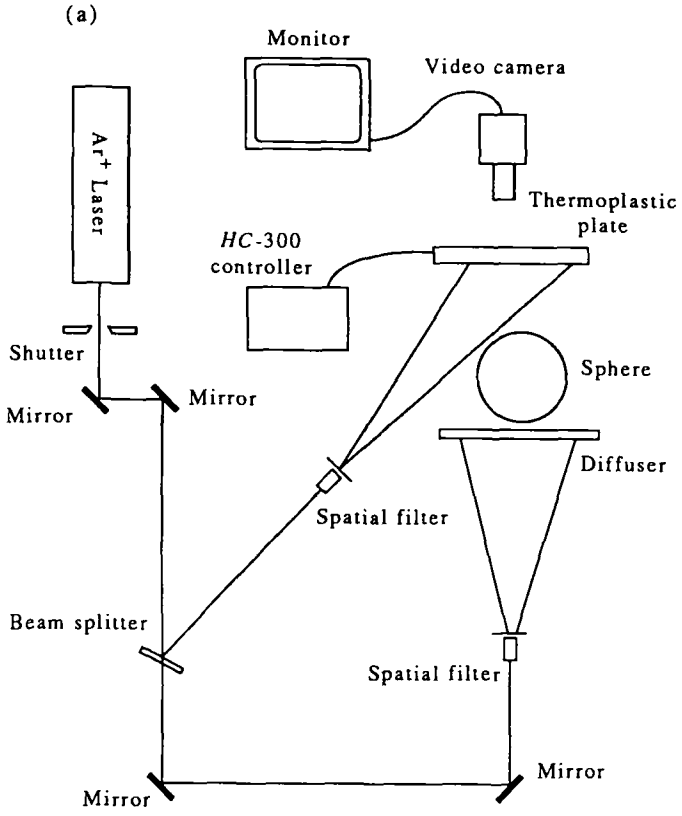

FIG. 2. (a) Layout of optical system: real time holographic interferometry; (b) photograph of optical system.

different types of convection that occurred at discrete Re during the real time evaluation (at $Re = 0$, 475, 3810, 5180 and 9065). A picture of the typical fringe pattern representing free convection ($Re = 0$, corresponding to the case of a stationary sphere) is shown in Fig. 5(a). Here, a flow current can be seen that originates in the lower portion of the sphere surface and extends to the upper, forming a steady plume. A similar free convection dominant flow with low rotational speed (about 100 rpm, $Re = 475$) is dis-

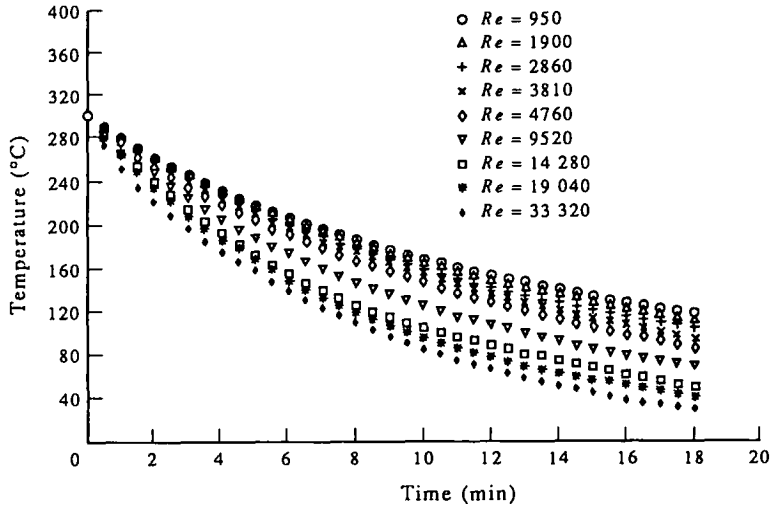

FIG. 3. Measured sphere temperatures as a function of time at different Reynolds numbers.

Table 1. Comparison of measured $\overline{Nu}$ with calculated $\overline{Nu}$ from equations (9) and (10)

Re	Gr^*	Gr/Re^2	Measured $\overline{Nu}$	Calculated $\overline{Nu}$ from equation (9)	Calculated $\overline{Nu}$ from equation (10)
250	3.07×10^5	4.91	24.10	5.90	16.36
	3.21×10^5	5.13	24.18		16.35
475	3.07×10^5	1.36	24.52	8.16	17.38
	3.21×10^5	1.42	24.21		17.36
950	3.07×10^5	0.34	24.87	11.62	19.88
	3.21×10^5	0.36	24.16		19.90
1200	3.07×10^5	0.21	25.81	13.51	21.12
	3.21×10^5	0.21	25.60		21.14
1900	3.07×10^5	0.085	26.60	16.44	24.11
	3.21×10^5	0.088	26.86		24.12
2860	3.07×10^5	0.037	28.60	20.16	27.37
	3.21×10^5	0.039	27.17		27.38
3810	3.07×10^5	0.021	29.35	23.28	29.99
	3.21×10^5	0.022	28.88		30.00
4760	3.07×10^5	0.013	31.83	26.02	32.22
	3.21×10^5	0.014	31.30		32.23
5810	3.07×10^5	0.0090	35.12	28.57	34.38
	3.21×10^5	0.0095	35.32		34.49
9520	3.07×10^5	0.0034	38.80	36.79	40.29
	3.21×10^5	0.0035	37.84		40.39
14280	3.07×10^5	0.0015	44.76	45.06	46.12
	3.21×10^5	0.0016	42.27		46.22
19040	3.07×10^5	0.0008	51.22	52.04	50.40
	3.21×10^5	0.0009	52.82		50.68
33320	3.07×10^5	0.0003	69.62	68.84	60.67
	3.21×10^5	0.0003	68.43		60.88

played in Fig. 5(b), but here the thermal plume is slightly broader and distorted. Essentially, the thermal boundary layer introduced mainly by the buoyancy force around the sphere surface (see Figs. 5(a) and (b)) transfers heat energy by a slow fluid motion. Since the real time holographic visualizations revealed that neither the flow patterns, nor the thickness of thermal boundary layer changed to a significant degree in the range $Re < 1000$, the buoyancy effect must be dominant; the centrifugal effect being rather weak. Thus,

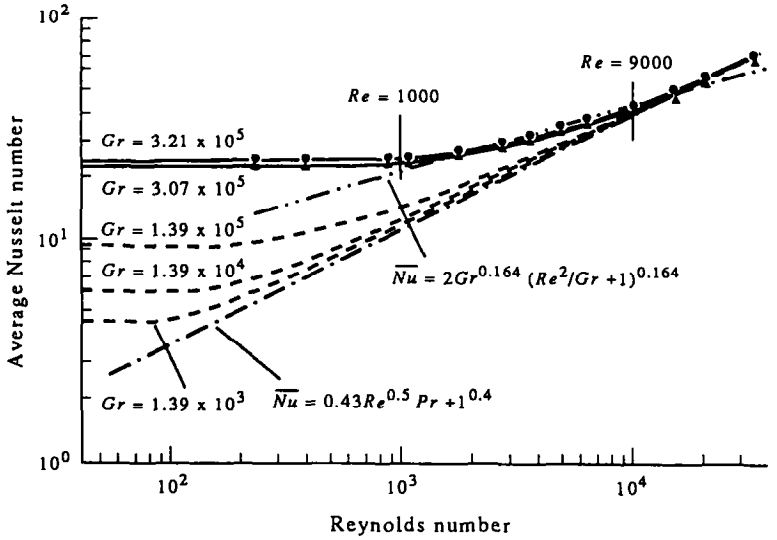

FIG. 4. Average Nusselt number as a function of Reynolds number. (●) Measured data for $Gr = 3.21 \times 10^5$; (▲) measured data for $Gr = 3.07 \times 10^5$; (----) predictions of Farouk [2]; (—·—) empirical correlation by Kreith *et al.* [9]; (—··—) empirical correlation by Nordlie and Kreith [11].

heat transfer is attributable mainly to free convection which results in a slowly increasing $\overline{Nu}$ as evidenced by Fig. 4.

However, as Re increases and the buoyancy parameter Gr/Re^2 decreases, centrifugal and buoyancy effects become comparable. At this point, according to the real time holographic observations, the convective flow begins to get complicated. In the range of $1000 < Re < 9000$, the flow pattern gradually undergoes remarkable changes, as the upward plume, which appeared at very low rotating speeds, becomes severely distorted and a previously unreported irregular and unsteady turbulent zone forms in the upper half of the sphere [14] (see Figs. 5(c) and (d)). Although the exact reason is not clear, the preliminary physical understanding given below perhaps can reasonably describe this phenomenon. For any heated rotating sphere, two flow currents exist; Stoke's centrifugal current [1], and another flow current arising from the buoyancy force, as shown in Fig. 6. The two flow currents move in the same direction on the lower half of the sphere, but in opposite directions on the upper half. For slower rotational speeds, the downward flow current (centrifugal) on the upper half of the sphere is weaker than the buoyancy current which forms the upward thermal plume shown in Figs. 5(a) and (b). If the strength of the centrifugal effect becomes comparable with that of the buoyancy current, which occurs as the rotational speed is increased, the two opposite flow currents on the upper half of the sphere come into collision, generating a very complex turbulent flow characterized by unsteady vortices. In addition, though weaker and narrower, an eruption jet located near the equatorial plane was also seen in this convection regime (see Fig. 5(d)). Obviously, in this regime, the flow around the sphere is a result of the interactions between the buoyancy and centrifugal effects which cause free and forced convection, respectively. Therefore, the regime between $1000 < Re < 9000$ belongs to free and forced mixed convection, in which the heat energy of the sphere is dissipated by complicated mixed convection rather than by simple free or forced convection. Furthermore, irregular eddying or crosswise mixing in the turbulent zone assists in improving heat transfer between the fluid and the surface of the rotating sphere. It was also noted that the area covered by the turbulent zone grows with increasing Re, which in combination with the complex flow structure in this regime will affect the heat transfer in a very complex manner, probably resulting in the gradual increase in $\overline{Nu}$ between $1000 < Re < 9000$, as evidenced in Fig. 4.

It was also noted from the real time observations, that the eruption jet became broader and stronger as Re increased, but that the irregular vortices in the turbulent zone gradually became more and more unclear after $Re = 9000$ (see Fig. 5(e)), and finally disappeared as Re approached about 15000. These phenomena demonstrate that the centrifugal effect becomes much stronger than the buoyancy effect when $Re > 9000$. Therefore, in this regime, forced convection becomes dominant, in which the heat energy is transferred very quickly by the strongest jet flow near the equatorial plane, resulting in an $\overline{Nu}$ that increases at a fast and linear rate with increasing Re.

It should be pointed out that no case above $Gr = 1.39 \times 10^5$ was studied in Farouk's work [2],

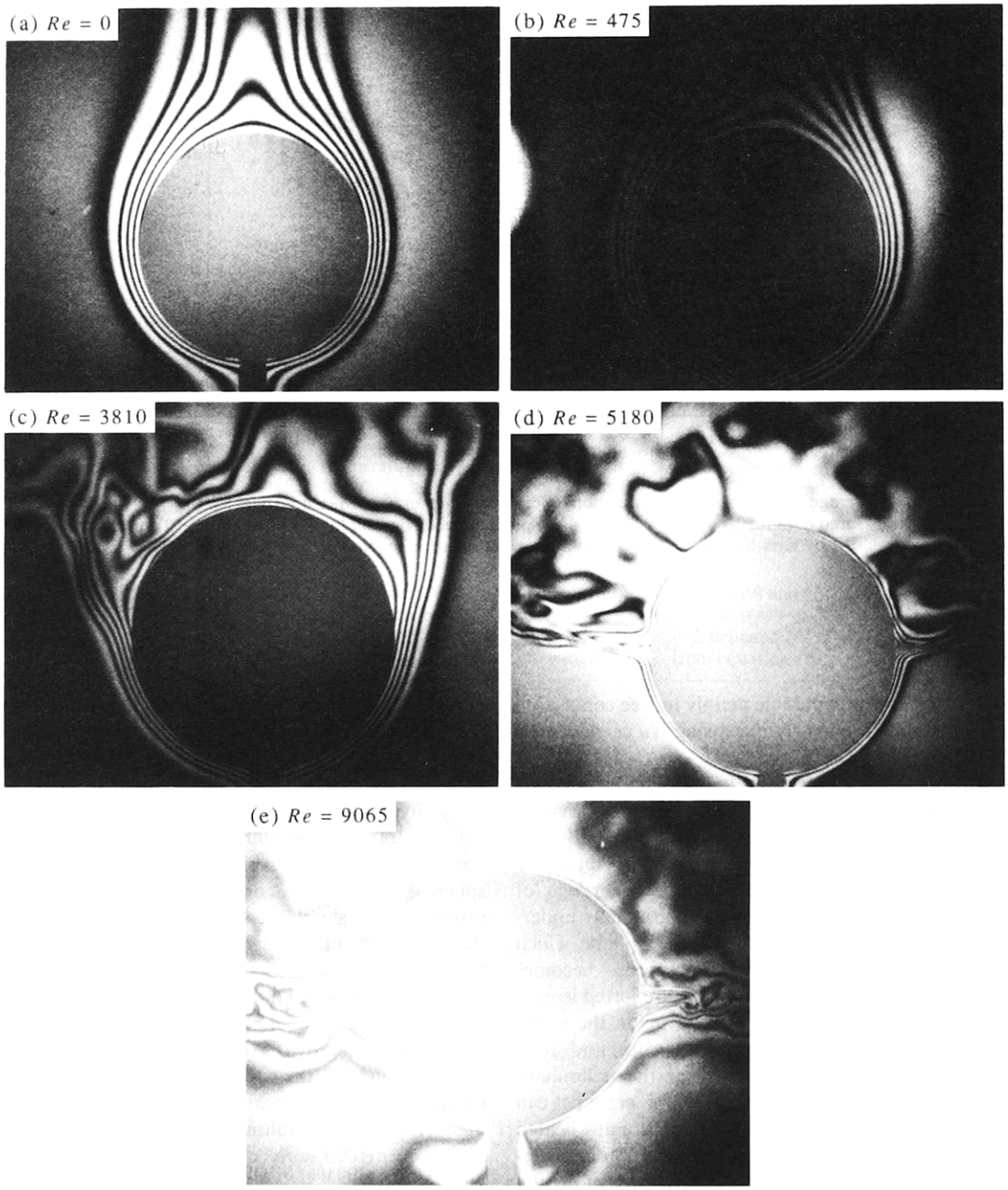

FIG. 5. Real time holographic visualization pictures of convective thermal flow around an isothermal rotating sphere at different Reynolds numbers.

since based on the analysis of Cremers and Finley [20] flow around even a stationary sphere was expected to be turbulent for $Gr > 1.39 \times 10^5$. In this experiment even though Gr values reached as high as 3.21×10^5, according to the real time holographic visualizations turbulent flow was not achieved as predicted by Cremers and Finley, but rather laminar flow persisted, even for a $Re = 1000$.

As mentioned in the Introduction, the correlation of $\overline{Nu}$ with other parameters has been studied by many authors. A comparison (listed in Table 1 and shown in Fig. 7) of the measured data with the empirical correlation obtained by Kreith *et al.* [9]

$$\overline{Nu} = 0.43 Re^{0.5} Pr^{0.4} \begin{cases} Re < 5 \times 10^5 \\ 0.7 < Pr < 217 \\ Gr/Re^2 < 0.1 \end{cases} \quad (9)$$

revealed considerable deviation in the range of $Re < 6000$. Kreith *et al.* [9] assumed that normal free convection was negligible for $Gr/Re^2 < 0.1$ (i.e. $Re > 1800$); the flow around the sphere being forced

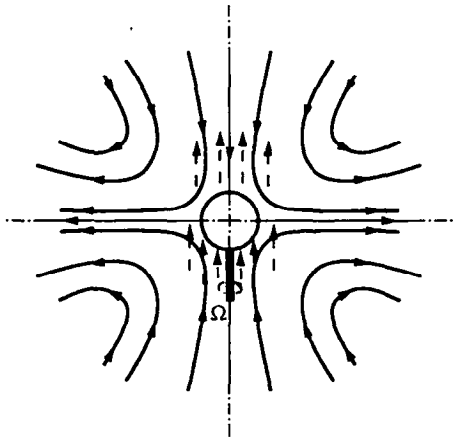

FIG. 6. Interaction between centrifugal current and buoyancy current.

convection, and thus the buoyancy parameter (Gr) is not considered in equation (9). However, as discussed above, the buoyancy effect cannot simply be ignored in this regime. Since between $1000 < Re < 9000$, the mixed convection flow around the sphere is the result of both centrifugal and buoyancy effects. The turbulent zone that appears in the mixed convection regime transfers much more energy than pure forced convection in the same operating range. This is perhaps one reason to explain the deviation in the range of $Re < 6000$. In addition, the correlation in equation (9) was obtained using a sphere rotating in oil and water (see Fig. 7) rather than air, as in the present experiment. This difference in media may also play a role in creating the deviation. Whether a turbulent zone, similar to that in the mixed convection regime described above, exists for a heated sphere rotating in an oil or water medium, was difficult to verify by present real time holographic observation.

The fact that between $1000 < Re < 9000$ mixed convection was dominant was further verified by a comparison of the measured data with Nordlie and Kreith's correlation for mixed convection [11]

$$\overline{Nu} = 2Gr^{0.164}\left(\frac{Re^2}{Gr}+1\right)^{0.164} \quad \begin{cases} 1\times10^3 < Re < 2\times10^4 \\ Gr/Re^2 > 0.1 \\ 4\times10^6 < Gr < 2\times10^7 \end{cases} \quad (10)$$

This correlation considers not only Re, but also Gr, i.e. not only the centrifugal but also the buoyancy effect. As evidenced in Fig. 8, the measured data in the mixed convection region between $1000 < Re < 9000$, at $Re = 1900, 2860, 3810, 4760, 5810$ and 9502, are in good agreement with the calculated values, but in the range $Gr/Re^2 > 0.3$ and $Gr/Re^2 < 0.004$ (i.e. $Re < 1000$ and $Re > 9000$, respectively), deviations exist. This comparison implies that the mixed convective range applicable to equation (10) (i.e. $Gr/Re^2 > 0.1$) is quite different from that obtained by this experiment (i.e. the range of $1000 < Re < 9000$, corresponding to $0.3 > Gr/Re^2 > 0.004$). Whether this fact indicated that the operating range for correlation (10) should be extended or corrected is not clear yet.

A better correlation was established according to Churchill's method [12], which proposed that the mixed convection around a rotating sphere can be considered a resultant effect composed of free and forced convection. Thus, the overall Nusselt number can be represented by

$$\overline{Nu}^3 = \overline{Nu}_N^3 + \overline{Nu}_F^3 \quad (1 < Gr < 10^5) \quad (11)$$

where $\overline{Nu}_N$ and $\overline{Nu}_F$ represent the average Nusselt number for free and forced convection, respectively, and are given by

$$\overline{Nu}_N = 2+0.392Gr^{0.25} \quad (1 < Gr < 10^5) \quad (12)$$

$$\overline{Nu}_F = 2+0.175Re^{0.583} \quad \begin{cases} Gr = 0.0 \\ 10 < Re < 10^4 \\ Pr = 0.721 \end{cases} \quad (13)$$

Large discrepancies were found between the measured data and the calculated values of equations (11)–(13). But note that equation (11) is only valid in the range $Gr < 10^5$, whereas the experiment employed Gr values greater than 3×10^5. Obviously the experimental buoyancy effect was much stronger than that in equation (11). Therefore, the power index of Gr in equation (12) should be increased in order to enhance the buoyancy effect, and was found to be 0.31; thus

$$\overline{Nu}_N = 2+0.392Gr^{0.31}. \quad (14)$$

Incorporating equation (14) into equation (11) yields an asymptotic relation that now correlates with the experimental data very well, as evidenced by Fig. 9. Clearly, between $1000 < Re < 9000$ the calculated curve correlated with the measured data in the mixed convection regime very well, while for $Re > 9000$ and $Re < 1000$, the forced ($\overline{Nu}_F$) and free ($\overline{Nu}_N$) convection regimes, respectively, are represented by the straight lines of the asymptotics.

The major source of error affecting the accuracy of the measured data (dT_s/dt) lies in the sphere's conductive heat loss along the rotational shaft. By taking into consideration the factors of heat conductivity as well as the surface area of the rotating shaft, an estimated error of about 3–4% could be introduced in this way.

Another possible source of error is the inertial time of the thermocouple for transient temperature measurements. This time depends on the heat capacitance of the thermocouple junction and the heat conductance from the sphere to the junction. However, due to the very small junction diameter ($\sim$0.1 mm)

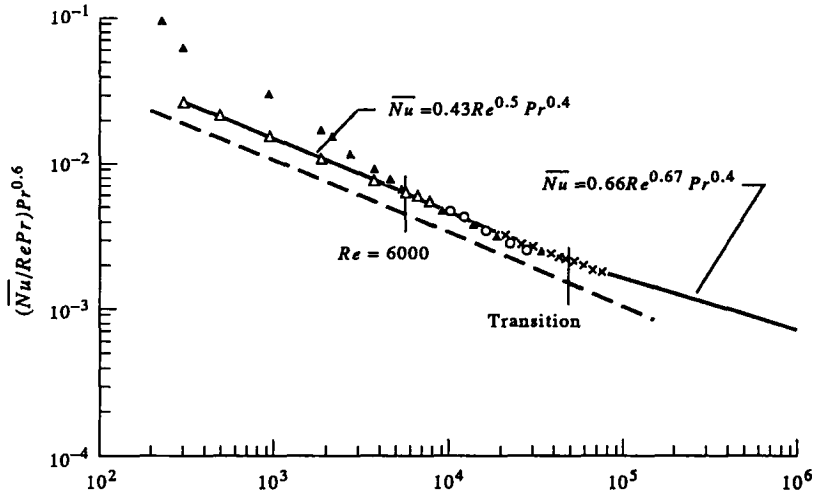

FIG. 7. Comparison of measured $\overline{Nu}$ with the empirical correlation of Kreith *et al.* [9]. (▲) Measured data for $Gr = 3.21 \times 10^5$ (present work; in air); (△) measured data of Kreith *et al.* [9] (in oil); (○) measured data of Kreith *et al.* [9] (in water); (×) measured data of Kreith *et al.* [9] (in air); (—) empirical correlation of Kreith *et al.* [9]; (— — —) theoretical prediction by Dorfman and Serazetdinov [8].

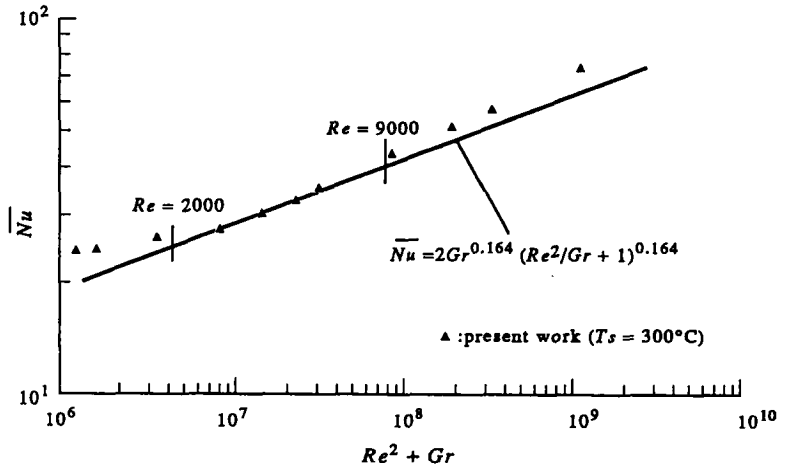

FIG. 8. Comparison of measured $\overline{Nu}$ with the empirical correlation of Nordlie and Kreith [11].

and exceedingly narrow gap-width (~1 mm) between the hole wall and the junction surface, the effect of the inertial time on dT_s/dt measurements is not significant. In terms of Newton's law of cooling and Black's heat capacity equation [21], the inertial time, in the case of the stationary sphere, was estimated to be 1.5 s. Note that an inertial time of this magnitude only introduces a temperature deviation of about 2°C at the measurement point $T_s = 300$°C. By taking account of the difference in slopes of the cooling curve data (see Fig. 3) (at 300 and 298°C), about 1–2% error in dT_s/dt is estimated due to the 2°C temperature deviation.

Furthermore, for the case of a rotating sphere, since a larger heat conductance from the sphere to the junction and thus a shorter inertial time are expected, an error of no more than 2% should be estimated.

The reason for the omission of radiative heat transfer in this experiment is given below. The radiation heat transfer coefficient can be expressed in the following form [9]

$$\bar{h}_r = \varepsilon\sigma(T_s^2+T_\infty^2)(T_s+T_\infty)$$

where $\sigma = 5.67 \times 10^{-8}$ W m^{-2} K^{-4} is the Stefan–Boltzman radiation constant; ε is the emissivity of the chrome steel sphere, which depends on the sphere substance, surface characteristics and temperature. For a polished chrome steel sphere surface at

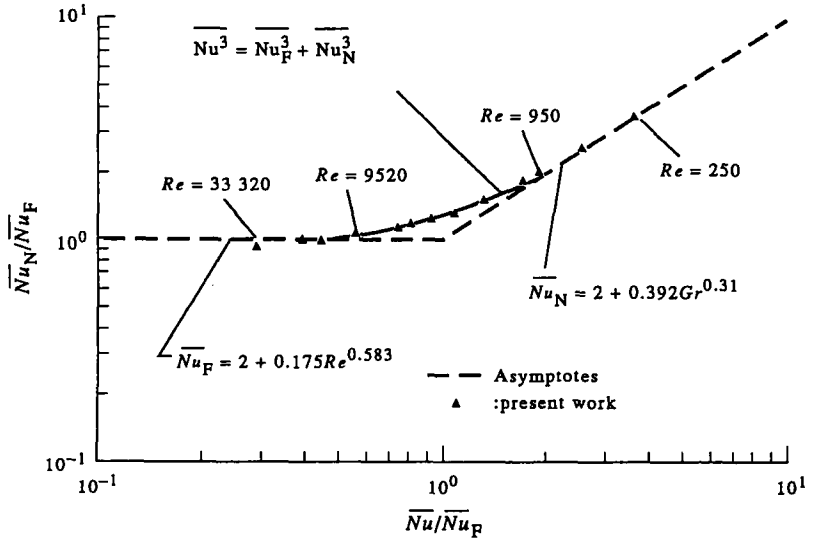

FIG. 9. New asymptotic formula for correlating measured $\overline{Nu}$.

$T = 300°C$, the emissivity is very low (less than 0.02). This corresponds to an $\bar{h}_r$ of 0.4 W m^{-2} K^{-1}, which is about 1.6% of the $\bar{h}_c$ value for a stationary sphere, and 0.6% for a sphere rotating at $Re = 33\,320$. Therefore its effect on the dT_s/dt measurement was not significant and was neglected in our measurement.

Note that heat loss by thermal conduction along the thermocouple leads also affects the measurement accuracy. This effect has been studied in detail by Bradley and Matthews [22], who showed that the error in temperature is smaller than 0.1% for wire leads of 12.5 μm in diameter and 0.3 cm in length. Note that Bradley and Matthews concluded that wires larger than 0.3 cm in length would result in even lower errors in temperature. In our study, the diameter of the leads was 25 μm, while the length of those situated in the hole was longer than 0.3 cm ($\simeq 1.5$ cm). From this analysis the heat loss can be considered negligible ($<0.1\%$).

For Re measurements, accuracy depends mainly on the rotational speed measurement equipment used. An error of 5% at 1000 rpm was attributed to this equipment.

Although a vertical rotation axis was used in the experimental investigation, deviations from the vertical were also examined in order to determine the influence of small errors in the rotational angle upon the test results. The consistency of the results, however, indicated that these effects were small enough to be ignored.

4. CONCLUSION

The average Nusselt number of a heated sphere rotating in air was measured experimentally over a wide range of Re from 0 to 33 320 ($Gr \approx 3 \times 10^5$). As well, the evolution of the flow structure was observed by real time holographic interferometry.

The exhibited $\overline{Nu}$ behavior was in good agreement with the theoretical predictions of Farouk [2], and could be well explained by the flow visualization analysis. For $Re < 1000$, the buoyancy effect was dominant; the slow heat transfer being attributable mainly to free convection. In the range $1000 < Re < 9000$, the flow around the sphere was very complex, forming a free and forced mixed convection, characterized by a turbulent zone and an eruption jet which affect the heat transfer characteristics in a complicated manner. As a result, $\overline{Nu}$ was found to increase along a curved path (see Fig. 4). When $Re > 9000$, forced convection dominated, in which the stronger and wider eruption jet was the main cause of heat transfer, literally throwing the heat energy away from the sphere, and resulting in a fast and linearly increasing $\overline{Nu}$.

The deviations revealed by a comparison of the measured data $\overline{Nu}$ with the empirical correlations of Kreith *et al.* [9], and Nordlie and Kreith [11], were shown to result from the effects of the flow structure in the evolution process around the rotating sphere.

Furthermore, following Churchill's method [12], a new asymptotic formula for correlating the measured data $\overline{Nu}$ was found

$$\begin{cases} \overline{Nu^3} = \overline{Nu_N^3} + \overline{Nu_F^3} \\ \overline{Nu}_N = 2 + 0.392Gr^{0.31} \quad (Gr > 3 \times 10^5) \\ \overline{Nu}_F = 2 + 0.175Re^{0.583} \begin{cases} Gr = 0.0 \\ Re < 33\,320 \\ Pr = 0.71 \end{cases} \end{cases}.$$

Acknowledgement—The authors gratefully acknowledge the financial support of this project by the National Science Council of the Republic of China under Contract No. NSC 80-0401-E-006-47.

REFERENCES

1. S. G. Stokes, On the theories of the internal friction of fluid in motion, *Camb. Trans.* **8,** 287 (1845).
2. B. Farouk, Mixed convective flow around a slowly rotating isothermal sphere, *Trans. ASME: J. Heat Transfer* **107,** 431–438 (1985).
3. F. S. Lien, C. K. Chen and J. W. Cleaver, Mixed and free convection over a rotating sphere with blowing and suction, *Trans. ASME: J. Heat Transfer* **108,** 398–404 (1986).
4. G. L. Palec and M. Daguenet, Laminar three-dimensional mixed convection about a rotating sphere in stream, *Int. J. Heat Mass Transfer* **30,** 1511–1523 (1987).
5. T. S. Chen and A. Mucoglu, Analysis of mixed forced and free convection about a sphere, *Int. J. Heat Mass Transfer* **20,** 867–875 (1977).
6. P. Hatzikonstantinou, Unsteady mixed convection about a porous rotating sphere, *Int. J. Heat Mass Transfer* **33,** 19–27 (1990).
7. T. Yuge, Experiments on heat transfer from sphere including combined, natured and forced convection, *ASME Trans. Ser. C* **82,** 214–220 (1960).
8. L. A. Dorfman and A. Z. Serazetdinov, Laminar flow and heat transfer near rotating axisymmetric surface, *Int. J. Heat Mass Transfer* **8,** 317–327 (1965).
9. F. Kreith, L. G. Roberts, J. A. Sullivan and S. N. Sinha, Convection heat transfer and flow phenomena of rotating sphere, *Int. J. Heat Mass Transfer* **6,** 881–895 (1963).
10. W. H. H. Banks, The thermal laminar boundary layer on rotating sphere, *J. Appl. Math. Phys.* **16,** 780–788 (1965).
11. R. Nordlie and F. Kreith, Convection heat transfer from a rotating sphere, *International Development in Heat Transfer*, pp. 461–467. ASME, New York (1961).
12. S. W. Churchill, The development of theoretically based correlations for heat and mass transfer, *Proc. First Latin-American Conf. Heat Mass Transfer*, Laplata, Argentina, 2 November (1982).
13. F. Kreith, Convection heat transfer in rotating system, *Adv. Heat Transfer* **5,** 129–251 (1968).
14. S. M. Tieng and A. C. Yan, Investigation of mixed convection about a rotating sphere by holographic interferometry, *J. Thermophys. Heat Transfer* **6**(4), 727–732 (1992).
15. F. P. Incropera and D. P. Dewitt, *Fundamentals of Heat and Mass Transfer* (3rd Edn). Wiley, New York (1990).
16. Y. Bayazitoglu and M. N. Ötisik, *Elements of Heat Transfer*. McGraw-Hill, New York (1988).
17. W. M. Kays and M. E. Crawford, *Convective Heat and Mass Transfer*, p. 388. McGraw-Hill, New York (1980).
18. C. M. Vest, *Holographic Interferometry*. Wiley, New York (1979).
19. P. Hariharan, *Optical Holography*. Cambridge University Press, London (1984).
20. C. J. Cremers and D. L. Finley, Natural convection about isothermal sphere, *Proc. 4th Int. Heat Transfer Conf.*, Paris, Vol. 4, pp. 6–15. Hemisphere, Washington, D.C. (1970).
21. R. P. Benedict, *Fundamentals of Temperature, Pressure, and Flow Measurement* (3rd Edn). Wiley, New York (1984).
22. D. Bradley and K. J. Matthews, Measurement of high gas temperature with fine wire thermocouples, *J. Mech. Engng Sci.* **10,** 708–711 (1968).